Mol Divers (2010) 14:595–604
DOI 10.1007/s11030-009-9172-6

FULL-LENGTH PAPER

In silico structure-based design of a novel class of potent and selective small peptide inhibitor of *Mycobacterium tuberculosis* Dihydrofolate reductase, a potential target for anti-TB drug discovery

Manoj Kumar · Rajakrishnan Vijayakrishnan · Gita Subba Rao

Received: 27 January 2009 / Accepted: 29 May 2009 / Published online: 21 August 2009

Abstract The worldwide TB structural genomics initiative has identified several new drug targets for *Mycobacterium tuberculosis* (*M. tb*). Dihydrofolate reductase (DHFR) catalyzes the NADPH-dependent reduction of dihydrofolate to tetrahydrofolate that is essential for DNA synthesis. Inhibition of its activity leads to arrest of DNA synthesis and hence cell death. Thus, *M. tb* DHFR (*mt*DHFR) is an attractive novel drug target for developing anti-TB drugs. Structural comparison of *mt*DHFR and human DHFR (*h*DHFR) reveals key differences in the active sites. These differences can be exploited for the design of selective inhibitors for *mt*DHFR. Based on the recently determined high resolution crystal structure of *mt*DHFR complexed with known inhibitor methotrexate (MTX) and cofactor NADPH, a tri-peptide inhibitor has been identified using a structure-based drug design approach. Docking studies indicate that the designed tripeptide inhibitor has a high potency ($K_d = 1.78$ nM) and is a selective (approximately 120 fold over *h*DHFR) inhibitor for *mt*DHFR. Hence, the tripeptide is a suitable lead compound for the development of novel anti-TB drugs.

Keywords *M. tuberculosis* · Dihydrofolate reductase · Anti-TB drug · Structure-based drug design

M. Kumar · R. Vijayakrishnan · G. Subba Rao
Department of Biophysics, All India Institute of Medical Sciences, New Delhi 110029, India

G. Subba Rao (✉)
National Academy of Medical Sciences (India), Ansari Nagar, New Delhi 110029, India
e-mail: gitasubba@gmail.com

Introduction

Mycobacterium tuberculosis (*M. tb*), the main causative agent for TB in humans, is responsible for more deaths in the world today than any other single infectious agent [1]. Because of the lack of an effective vaccine, chemotherapy with four front line drugs (e.g., rifampicin, isoniazid, pyrazinamide, ethambutol) for six months is the only existing treatment regimen [2]. However, the rapid increase of multi-drug-resistant tuberculosis (MDR-TB) (resistant to at least isoniazid and rifampicin) and extensively drug-resistant tuberculosis (XDR-TB) (resistant to at least isoniazid and rifampicin and additionally to fluoroquinolone and kanamycin, amikacin, or capreomycin among second line anti-TB drugs) has led to an urgent need for the identification of new drug targets and the development of novel anti-TB drugs [3–5].

The enzyme dihydrofolate reductase (DHFR) catalyzes NADPH-dependent reduction of dihydrofolate to tetrahydrofolate which is a precursor of cofactors necessary for the synthesis of thymidylate, purine nucleotides, methionine, serine, and glycine required for DNA, RNA, and protein synthesis. Inhibition of DHFR leads to the arrest of DNA synthesis causing cell death. This inhibition is the basis of the use of methotrexate (MTX) in the cancer therapy [6]. However, MTX is not selective for *mt*DHFR [7]. The clinical drug trimethoprim (TMP) and pyrimethamine (PYR) are selective and potent inhibitors of bacterial and protozoal DHFR respectively [7,8], but TMP has low affinity for *M. tb* DHFR [7]. Triazine Br-WR99210 has been shown to be a potent inhibitor of malarial DHFR [9]. However, it has been used only as an experimental drug on account of its harmful side-effects. DHFR inhibitors (TMP and sulfamethoxazole) have been used in Cote d'Ivoire in the treatment of patients infected with both HIV and *M. tb* [10]. Recently, it has been shown that DHFR is also a target for the front-line drug isoniazid [11].

The low sequence identity of ∼26% between *h*DHFR and *mt*DHFR suggested possible differences in the crucial regions of the two enzymes. This has been confirmed by the high resolution crystal structures of *mt*DHFR and *h*DHFR in binary and ternary complexes with its cofactor NADPH and its inhibitors, MTX and N^{α}-(4-amino-4-deoxypteroyl)-N^{δ}-hemiphthloyl-L-ornithine (PT523), respectively [12–14]. PT523 is a non-polyglutamate analogue of MTX and has been reported to bind 10–100 fold more tightly than MTX to recombinant *h*DHFR [15]. The structural comparison of *mt*DHFR [PDB ID: 1DF7] [12] and *h*DHFR [PDB ID: 1OHJ] [14] is shown in Fig. 1a and b.

The overall fold of *mt*DHFR and *h*DHFR is similar. It consists of a central β-sheet flanked by four α-helices. This β-sheet is made up of seven parallel strands and a C-terminal anti-parallel strand. The structural comparison of *mt*DHFR [PDB ID: 1DF7] and *h*DHFR [PDB ID: 1OHJ] reveals striking differences in the NADPH, MTX, and PT523-binding sites, respectively. In particular, in the ternary complex of MTX with *mt*DHFR, a glycerol molecule (glycerol A) is found close to MTX in a pocket formed by Trp22, Asp27, and Gln28 (Fig. 2a) while in *h*DHFR, the glycerol-binding site is packed with three hydrophobic residue side chains, Leu22, Pro26, and Phe31 (Fig. 2b). These differences can be exploited for the design of a selective inhibitor for *mt*DHFR.

Thus, *mt*DHFR is an attractive target for the development of a novel class of anti-TB drugs. A set of 2,4-diamino-*S*-methyl-5-dazapteridine (DMDP) derivatives was recently proposed and shown to be selective inhibitors of *mt*DHFR [16]. Out of the 18 inhibitors studied, the best one had an activity of 23 nM and was 65-fold selective over *h*DHFR.

In an effort to identify more potent and selective inhibitors of *mt*DHFR, we have undertaken a study of small peptide inhibitors as potential lead compounds. Although peptides are generally known to have undesirable pharmacokinetic properties, yet they have provided novel lead compounds and, in several cases, modified peptide analogues have been developed as drugs. Also, with recent advances in the drug delivery techniques, the opportunities for peptide drug development have been significantly enhanced [17]. Based on the crystal structures of *mt*DHFR complexed with NADPH and MTX [PDB ID: 1DF7] and *h*DHFR complexed with NADPH and PT523 [PDB ID: 1OHJ], we have used a structure-based approach for designing a set of small peptides. Docking and scoring of these peptides using Discovery Studio (DS) 1.7 [18] have identified some of them to be more potent and more selective for *mt*DHFR as compared to the inhibitors proposed so far.

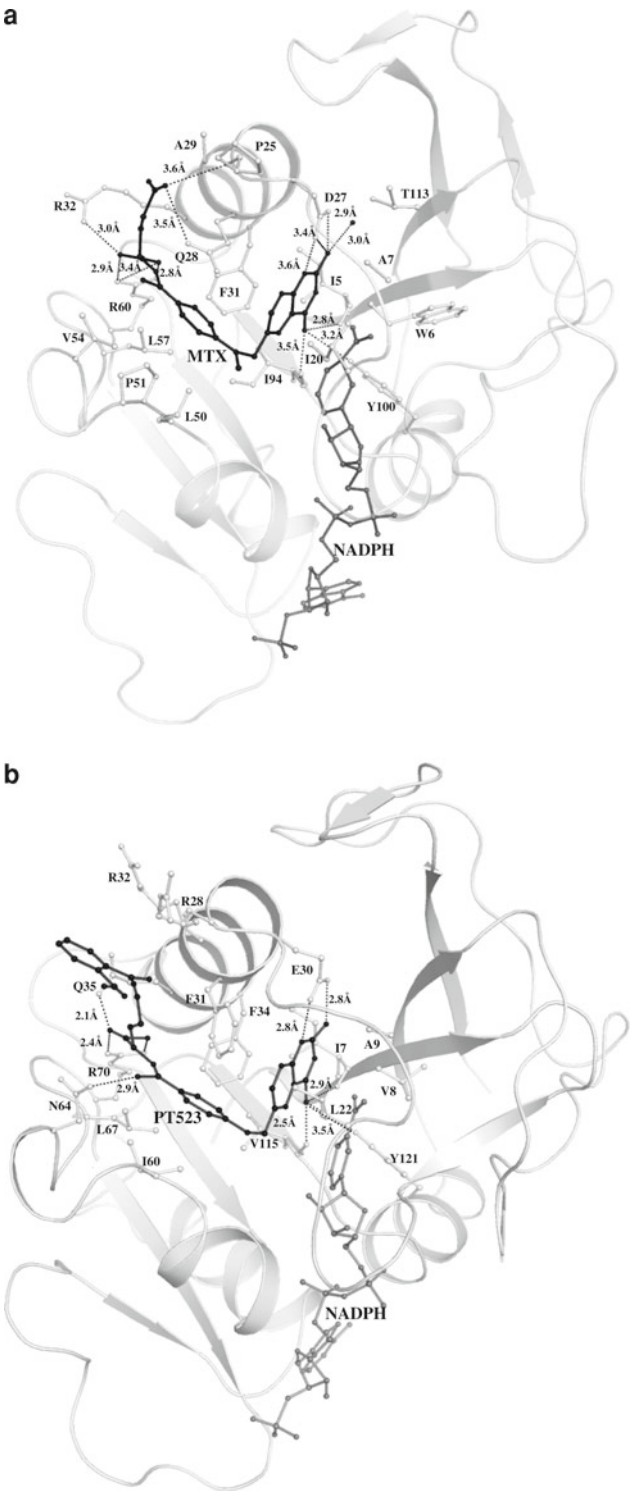

Fig. 1 Crystal structure of **a** *mt*DHFR (cartoon rendering in *grey*) complexed with MTX (in *black*, ball-and-stick rendering) and **b** *h*DHFR (cartoon rendering in *grey*) complexed with PT523 (in *black*, ball-and-stick rendering) showing the active site residues (ball and stick rendering in *grey*). Hydrogen bonds are shown as *black*, *dashed lines* together with distances. All the figures were produced using PyMol v0.99 [29]

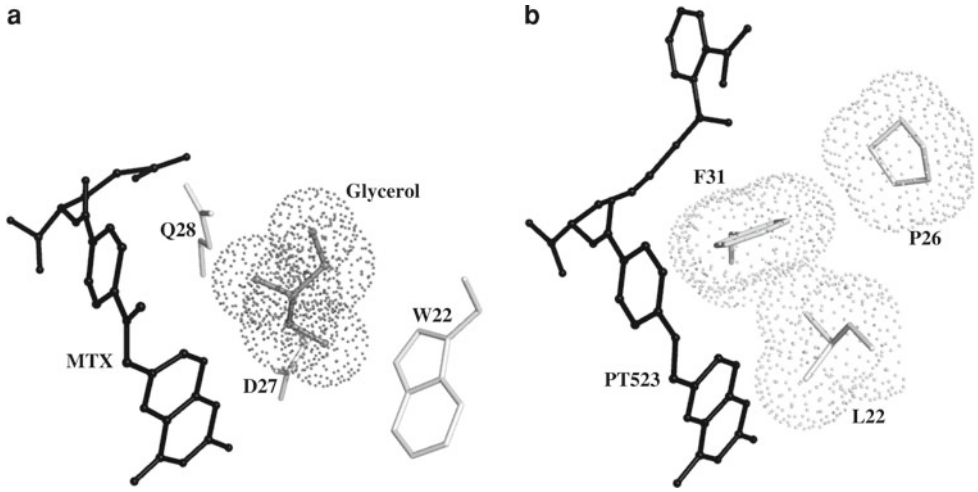

Fig. 2 Difference between binding sites of MTX and PT523 in *mt*DHFR and *h*DHFR, respectively. MTX and PT523 are shown as ball-and-stick rendering colored in black. Glycerol is shown as ball-and-stick rendering in *grey* surrounded by *grey dots* while side-chains of interacting residues are shown as stick rendering in *grey*

Materials and methods

The starting point for the computational studies was the X-ray crystal structure of *mt*DHFR complexed with the cofactor NADPH and MTX [PDB: ID 1DF7]. All computations were done using DS 1.7 [18].

Receptor setup

The target protein [PDB ID: 1DF7] was taken, the ligand MTX was extracted, hydrogens were added, and their positions were optimized using the all-atom CHARMm (version-c32b1) forcefield [19,20] and the Adopted Basis set Newton Raphson (ABNR) method available in DS 1.7 protocol until the root mean square (r.m.s.) gradient was less than 0.05 kcal/mol/Å. The minimized protein was defined as the receptor using the binding site module of DS 1.7. The binding site was defined from the volume of ligand method which was modified to accommodate all the important interacting residues in the active site of *mt*DHFR. The Input Site Sphere was defined over the binding site, with a radius of 5 Å from the center of the binding site. The protein, thus characterized, was taken as the target receptor for the docking procedure.

Ligand setup

Using the build-and-edit module of DS 1.7, a peptide of the desired sequence with a protonated amino group and a deprotonated carboxyl group was built, all-atom CHARMm forcefield parameterization was assigned and then minimized using the ABNR method as described above. A conformational search of the peptide was carried out using a simulated annealing molecular dynamics (MD) approach. The ligand was heated to a temperature of 700 K and then annealed to 200 K. Thirty such cycles were carried out. The conformation obtained at the end of each cycle was further subjected to local energy minimization, using the ABNR method as described above. The 30 energy-minimized structures were then superimposed and the lowest energy conformation occurring in the major cluster was taken to be the most probable conformation.

Docking and scoring

Docking of *mt*DHFR with the ligands was carried out with CDOCKER [21,22] protocol of DS 1.7. CDOCKER is a grid-based MD-simulated, annealing-based algorithm that uses CHARMm. The receptor (protein) is held rigid while the ligands are flexible during the refinement. The basic strategy involves the generation of several initial ligand orientations in the active site of the target protein followed by MD-based simulated annealing, and final refinement by minimization.

Input Site Sphere parameters specify a sphere around the center of the binding site, where the CDOCKER experiment is to be performed. The center of the Input Site Sphere is used for the initial ligand placement. Fifty replicas for each ligand are generated and randomly distributed around the center of the active site. Each of these is subjected to MD-based simulated annealing and final refinement by minimization, leading to 50 minimized docked poses.

The docked complexes are further refined by the Ligand Minimization protocol, during which the side-chain atoms within the Input Site Sphere are free to move. A Smart Minimizer algorithm with 1,000 steps and r.m.s. gradient of 0.05 kcal/mol/Å is used for ligand minimization.

The final step in docking is the scoring of the refined docked poses. This is done using the Score Ligand Poses protocol of DS 1.7. The Ludi Energy Estimate [23–25] was used for scoring the refined poses. The ligand pose which corresponded to the highest Ludi score [26] was taken as the best-docked pose.

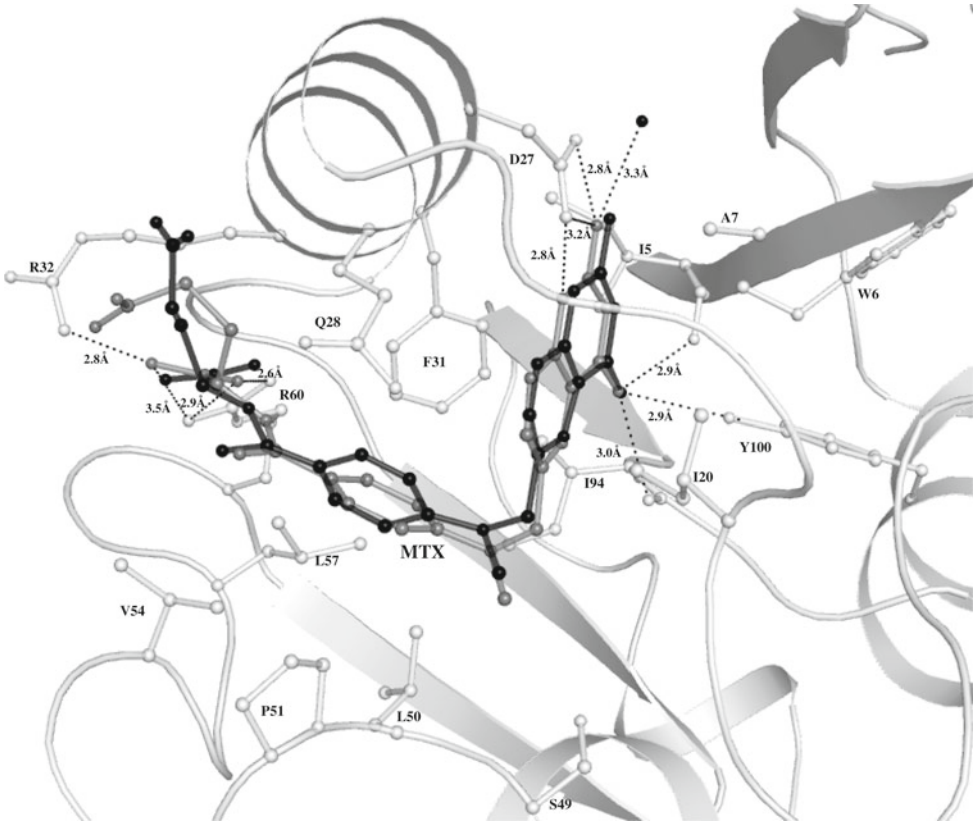

Fig. 3 Docked position of MTX (in *grey*) superimposed on the crystal structure position (in *black*). The coloring and rendering are the same as in Fig. 1

Molecular dynamics

In order to check whether the designed inhibitor remains bound in the presence of explicit solvent, a MD simulation was carried out on a fully hydrated model using explicit spherical boundary with harmonic restraint.

The final receptor–ligand complex was first solvated using the explicit solvent model mentioned above. The Standard Dynamics Cascade Protocol [27] of DS 1.7 was used with a time step of 1fs. The first step in the MD simulation was the energy minimization of the hydrated model during which the backbone of the refined receptor was kept fixed. The minimized hydrated complex was then subjected to a MD simulation in three stages. In the first stage, the temperature of the system was raised from 50 to 300 K over 2 ps. Next, the system was equilibrated for 20 ps, and finally the production run was carried out for another 150 ps.

Results and discussion

Validation of the docking methodology

The docking methodology was first tested on two known inhibitors (MTX and Br-WR99210), which were docked in the folate-binding site of *mt*DHFR, after extracting the ligand from the crystal structure.

Figure 3 shows the superimposition of the docked MTX (in grey) with the crystal structure position (in black). The structures are seen to overlap very well with a positional rmsd of 0.94 Å. The Ludi score is found to be 825, and the corresponding K_d value $\{-\log K_d = (\text{Ludi score}/100)\}$ is $5.6 \times 10^{-3}\,\mu M$. This is in good agreement with the observed value of $11 \times 10^{-3}\,\mu M$ [12].

Figure 4 shows the superimposition of the docked Br-WR99210 (in grey) with the crystal structure position (in black) [PDB ID: 1DG7] [12]. It can be seen that the two structures overlap very well with an rmsd of 0.60 Å. The predicted activity (K_d value) was found to be 1.0 μM, which agrees well with the experimental value of 0.19 μM [12].

The validation of the docking methodology was also carried out for the inhibitor PT523 complex with *h*DHFR. The results are shown in Fig. 5. Once again there is a good overlap of the docked PT523 (in grey) and the crystal structure position (in black). The predicted K_d value of $1.02 \times 10^{-5}\,\mu M$ agrees well with the observed value (reported to be a better inhibitor than MTX, which has a measured K_d value of $1.2 \times 10^{-3}\,\mu M$).

Thus, the above results provide a sound validation of the docking and scoring methodology used in this study.

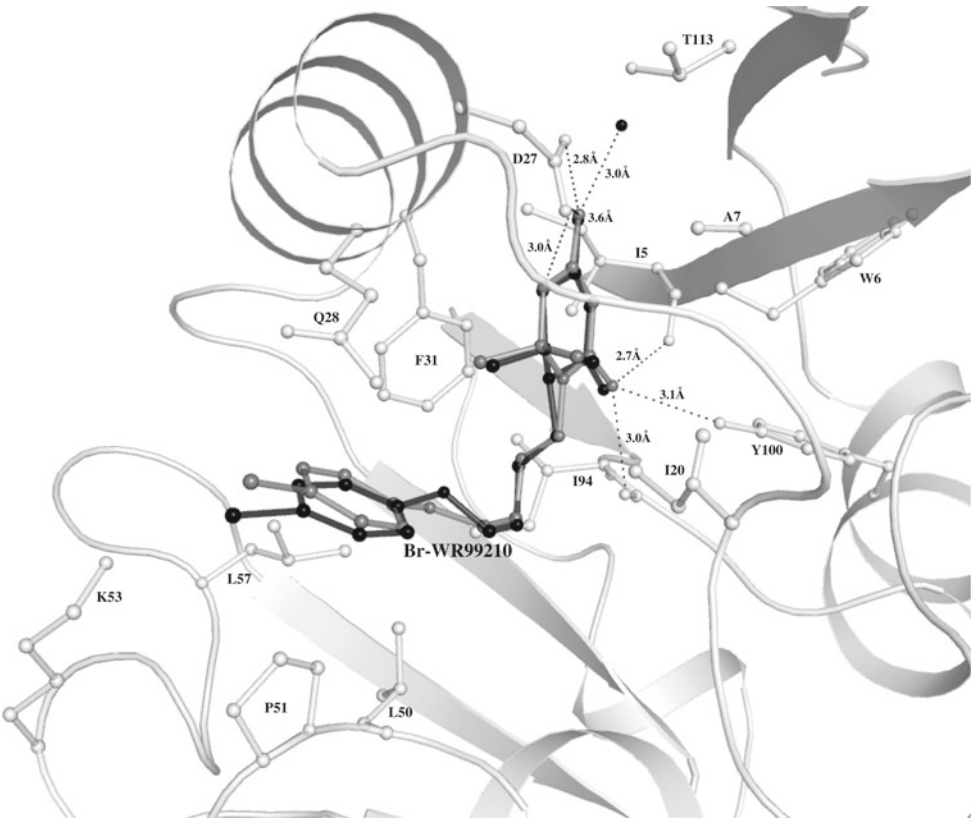

Fig. 4 Docked position of Br-WR99210 (in *grey*) superimposed on the crystal structure position (in *black*). The coloring and rendering are the same as in Fig. 1

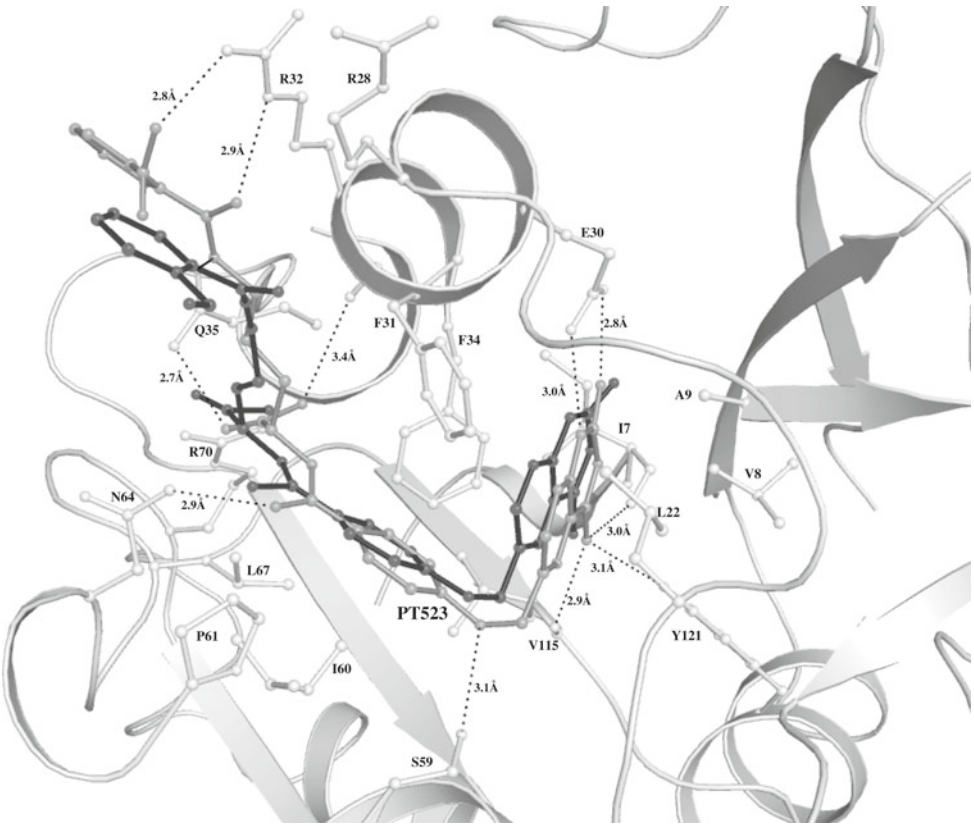

Fig. 5 Docked position of PT523 (in *grey*) superimposed on the crystal structure position (in *black*). The coloring and rendering are the same as in Fig. 1

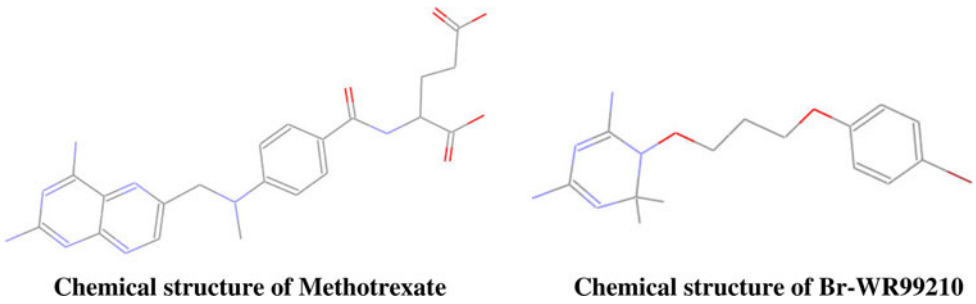

Fig. 6 Chemical structures of known inhibitors MTX and Br-WR99210

Table 1 Peptide sequences and their predicted activity

Peptide sequence	Predicted K_d value (M) for binding with	
	*mt*DHFR	*h*DHFR
WYD	1.26×10^{-7}	5.37×10^{-8}
WYE	5.02×10^{-6}	2.69×10^{-7}
WPD	9.12×10^{-9}	6.16×10^{-6}
WPE	1.02×10^{-6}	4.17×10^{-6}
YPD	4.17×10^{-8}	5.49×10^{-6}
YPE	2.75×10^{-8}	2.51×10^{-6}
WYY	$\mathbf{1.78 \times 10^{-9}}$	$\mathbf{2.09 \times 10^{-7}}$
WPY	9.55×10^{-8}	8.32×10^{-9}
WYP	4.57×10^{-8}	1.95×10^{-8}
WPW	4.27×10^{-6}	3.16×10^{-7}
WYW	1.45×10^{-7}	7.94×10^{-9}
WYS	1.44×10^{-8}	1.38×10^{-8}
WPS	7.94×10^{-8}	4.57×10^{-6}
WPT	2.95×10^{-7}	4.90×10^{-10}
WYT	3.31×10^{-6}	2.04×10^{-7}
YPS	8.91×10^{-6}	5.62×10^{-6}
YPT	6.46×10^{-6}	8.13×10^{-7}

Design of a peptide inhibitor and modeling of the docked complex of *mt*DHFR with the designed inhibitor

Based on the structures of the known inhibitors (Fig. 6), several tripeptide sequences containing two or three aromatic residues were designed and each of these tripeptides was docked after a conformational search as described in the methods. A list of trial sequences and the corresponding predicted activities is given in Table 1.

It can be seen that the tripeptide with the sequence

$$NH3^{+}-WYY-COO^{-}$$

has the highest activity with a K_d value of 1.7 nM.

The final docked position of the designed inhibitor is shown in Figs. 7 and 8, and the list of contacting residues (up to 4 Å) is given in Table 2. The tripeptide is seen to occupy a position similar to that of MTX, and in the vicinity of glycerol binding pocket. In addition, residue Y2 of the inhibitor is seen to have a close approach to NADP, making a hydrogen bond to NADP. The inhibitor is also hydrogen bonded to residue K53. These extra interactions are reflected in a lower docking energy as can be seen from Table 2.

Molecular dynamics simulation of a fully hydrated model of the final docked complex

The effect of solvent on the binding of the designed peptide inhibitor was studied by a MD simulation of a fully hydrated model as described in the methods. During the production phase of 150 ps following the initial heating and equilibration phases, the total energy and the simulation temperature were found to remain steady with little fluctuation. The snapshots of the dynamics trajectory at 25, 50, 75, 100, 125, and

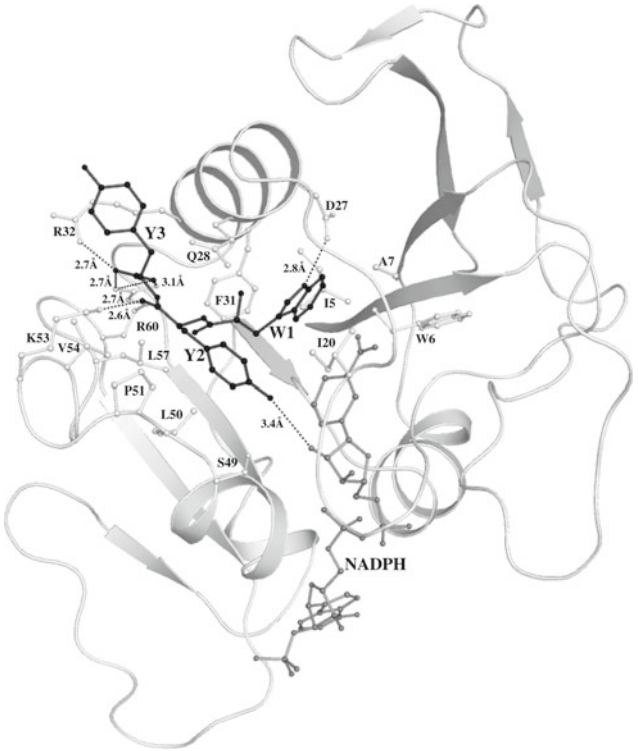

Fig. 7 Final docked position of the designed peptide inhibitor, WYY (*black*, ball-and-stick rendering) with *mt*DHFR. The coloring and rendering are the same as in Fig. 1

150 ps of the production run are shown in Fig. 9, while the corresponding interaction energies and interaction sets are given in Table 3.

The results indicate that the ligand as a whole moves into a more stable position with a much lower docked energy (Table 3). The residue Y2 of the inhibitor moves toward S49 of the enzyme, forming a hydrogen bond which is present throughout the simulation. The carbonyl group of Y2 which was initially hydrogen bonded to the residue K53 moves away and forms a hydrogen bond with Q28. W1 of the inhibitor, which was initially hydrogen bonded to D27, maintained so throughout the simulation. In addition, the ligand has van der Waals contacts with P58. The backbone of the ligand, which was allowed to vary in the simulation, is seen to remain fairly stable with hydrogen bonding to Q28 being retained throughout. The carboxy terminal of the ligand remains hydrogen bonded to R60 throughout the simulation. Thus, we have shown that the designed inhibitor remains bound in the presence of the explicit solvent.

Selectivity of the designed inhibitor

The selectivity of the designed peptide inhibitor for *mt*DHFR was checked by docking it with *h*DHFR [PDB ID: 1OHJ].

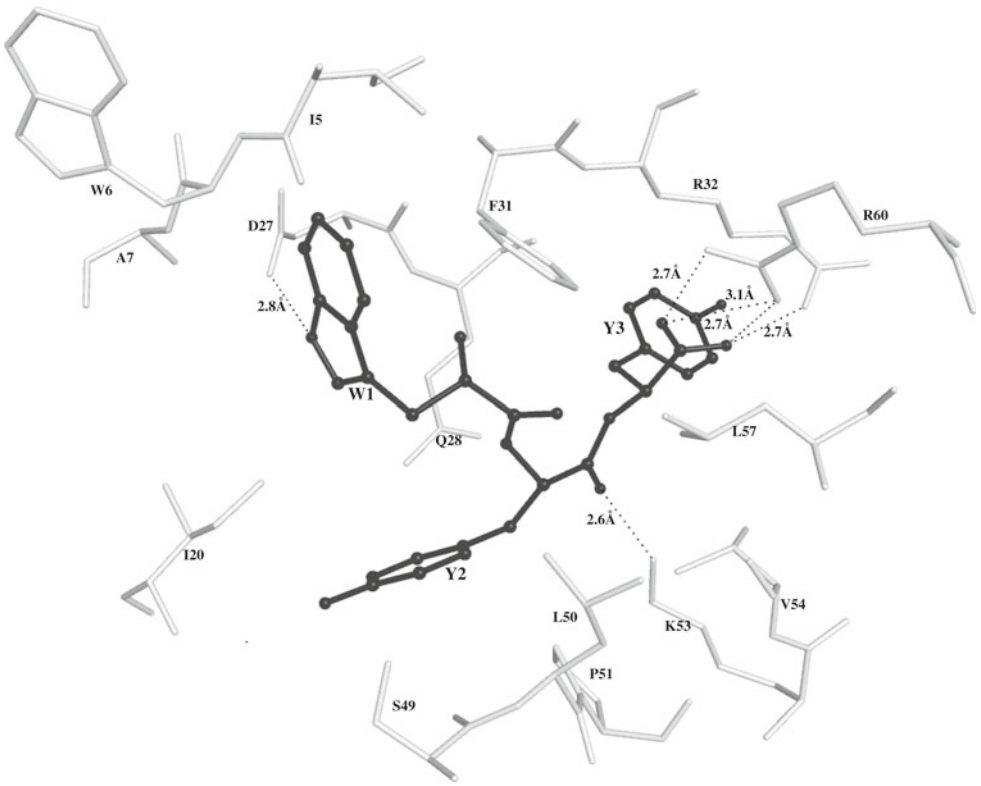

Fig. 8 Final docked complex of *mt*DHFR with the designed inhibitor, WYY. WYY is shown in *black*, ball-and-stick rendering, and the interacting side-chains of protein are shown as grey, stick rendering

Table 2 Discovery studio 1.7 docking results

Ligand	Docked energy (kcal mol^{-1})			Contacting residues (up to 4.0 Å) in final docked position
	Steric	Electrostatic	Total	
MTX	−51.19	−46.12	−97.31	**I5**, W6, A7, I20, **D27**, Q28, F31, **R32**, S49, L50, P51, V54, L57, **R60**, **I94**, **Y100**, NADPH, **H_2O**
Br-WR99210	−42.82	−25.06	−67.88	**I5**, W6**,** A7, I20, **D27**, Q28, F31, L50, P51, K53, L57, **I94**, **Y100**, T113, NADPH, **H_2O**
WYY	−50.34	−121.01	−171.35	I5, W6, A7, I20, **D27**, Q28, F31, **R32**, S49, L50, P51, **K53**, V54, L57, **R60**, **NADPH**

Hydrogen bonded residues are highlighted in bold

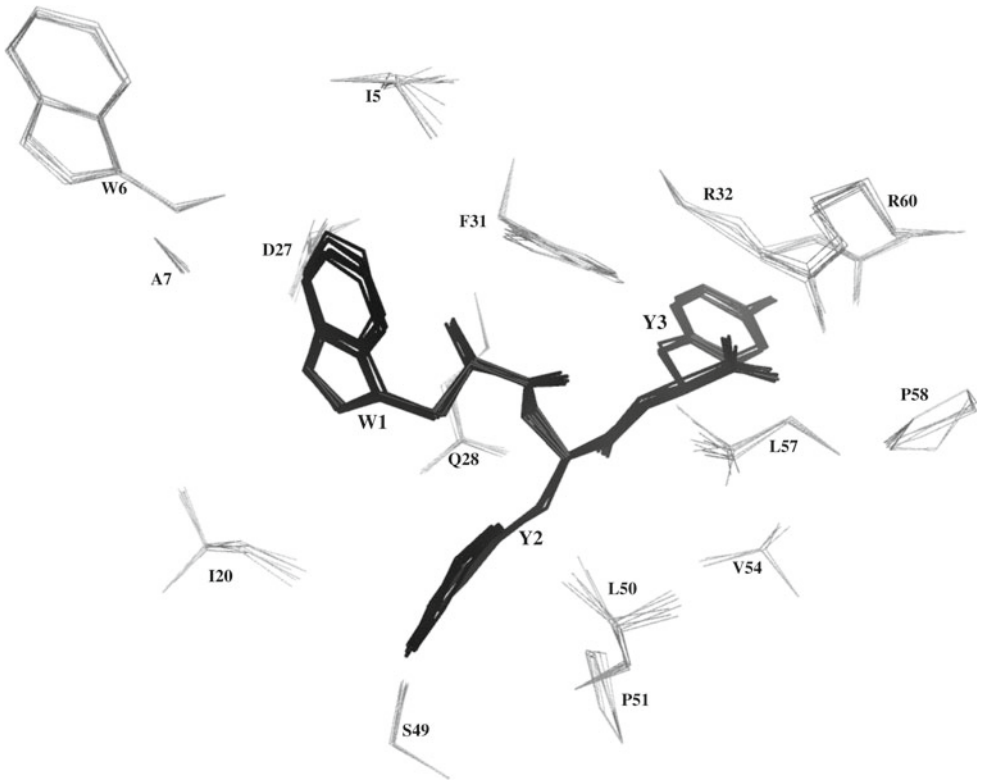

Fig. 9 Molecular dynamics trajectory for the docked complex. Snapshots of the designed peptide and the selected *mt*DHFR active site residue conformers extracted from the production dynamics trajectory at the time intervals of 0, 25, 50, 75, 100, 125, and 150 ps. The peptide is shown in *black* and the InhA residues are shown as *thin sticks in grey*. (NADPH has not been shown for the sake of clarity)

The docked complex is shown in Fig. 10. It can be seen from the Fig. 10 that designed inhibitor occupies a position similar to that in *mt*DHFR (Fig. 7). However, docking energy is higher (−120.54 kcal mol^{-1}), and the predicted K_d value is 0.21 μM. Thus, the modeling studies predict the tripeptide WYY to be about 120-fold selective for *mt*DHFR over *h*DHFR (Table 4).

Conclusion

Using an *in silico* structure-based approach, we have exploited the structural differences between *mt*DHFR and *h* DHFR to design a potent and selective small peptide inhibitor of *mt*DHFR. Docking studies indicate that the designed peptide has potency about six times that of the most potent,

Table 3 Fully hydrated dynamics simulation results of docked complex DHFR–WYY

Time (ps)	Docked Energy of ligand (kcal mol^{-1}						Contacting residues (upto 4.0 Å)
	With solvent and enzyme			With enzyme only			
	Steric	Electrostatic	Total	Steric	Electrostatic	Total	
0	−56.57	−657.22	−713.79	−45.58	−456.26	−501.84	I5, W6, A7, I20, **D27**, **Q28**, F31, **R32**, **S49**, L50, P51,V54, L57, P58, **R60**, I94, NADPH
25	−67.88	−650.95	−718.83	−55.34	−454.14	−509.48	I5, W6, A7, I20, **D27**, **Q28**, F31, **R32**, **S49**, L50, P51, L57, P58, **R60**, NADPH
50	−60.66	−650.32	−710.98	−48.38	−452.37	−500.75	I5, W6, A7, I20, **D27**, **Q28**, F31, **R32**, **S49**, L50, P51, V54, L57, P58, **R60**, NADPH
75	−56.50	−683.72	−740.22	−44.80	−459.18	−503.98	I5, W6, A7, I20, **D27**, **Q28**, F31, **R32**, **S49**, L50, P51,V54, L57, P58, **R60**, NADPH, H_2O
100	−57.43	−662.76	−720.19	−46.84	−463.03	−509.87	I5, W6, A7, I20, **D27**, **Q28**, F31, **R32**, **S49**, L50, P51, L57 P58, **R60**, NADPH
125	−59.31	−682.31	−741.62	−48.48	−467.13	−515.61	I5, W6, A7, I20, **D27**, **Q28**, F31, **R32**, **S49**, L50, P51, L57, **R60**, NADPH
150	−60.78	−674.82	−735.60	−48.37	−469.21	−517.58	I5, W6, A7, I20, **D27**, **Q28**, F31, **R32**, **S49**, L50, P51,V54, L57, P58, **R60**, NADPH

Hydrogen bonded residues are highlighted in bold

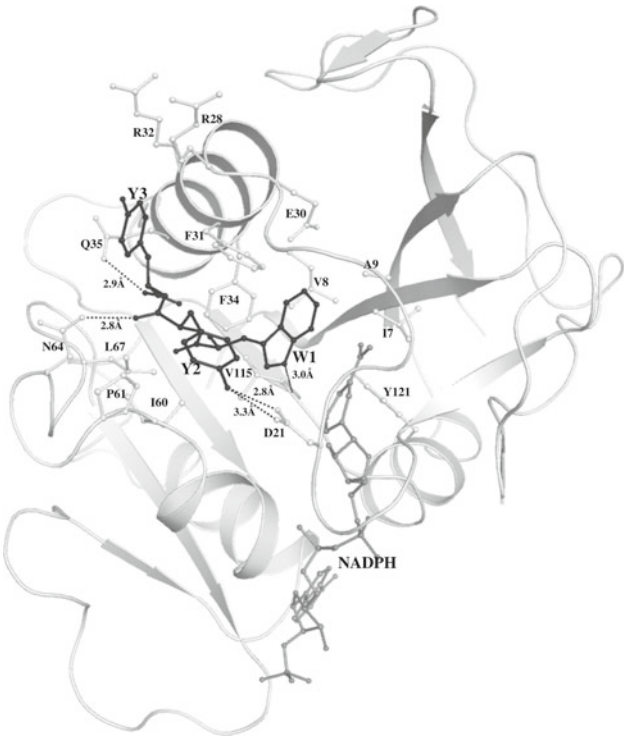

Fig. 10 Final docked position of the designed peptide inhibitor, WYY (*black*, ball-and-stick rendering) with *h*DHFR. The coloring and rendering are the same as in Fig. 1

known inhibitor (MTX), and is about 120 fold selective for *mt* DHFR over *h* DHFR. Thus, the designed tripeptide, WYY, is a suitable lead compound for the development of a new class of selective drugs for anti-tubercular therapy. A similar approach has been adopted by us earlier [28] for designing a small peptide inhibitor of NADH-dependent Enoyl-ACP reductase (InhA).

Table 4 Selectivity of designed ligand (WYY)

	Target	Corresponding K_d value at 298 K (nM)	Selectivity ratio
1	*mt*DHFR	1.78	1
2	*h*DHFR	209	117.4

References

1. Tuberculosis (as of 17 March 2009) -> Estimated TB -> Estimated TB deaths (MDG indicator 23). WHO Global Tuberculosis Database
2. Chan ED, Iseman MD (2002) Current medical treatment for tuberculosis. Br Med J 325:1282–1286
3. Corbett EL, Watt CJ, Walker N, Maher D, Williams BG, Raviglione MC, Dye C (2003) The growing burden of tuberculosis: global trends and interactions with the HIV epidemic. Arch Intern Med 163:1009–1021
4. Nachega JB, Chaisson RE (2003) Tuberculosis drug resistance: a global threat. Clin Infect Dis 36(Suppl 1):S24–S30
5. Raviglione M, Smith I (2007) XDR tuberculosis—implications for global public health. N Engl J Med 356((7):656–659
6. Schweitzer BI, Dicker AP, Bertino JR (1990) Dihydrofolate reductase as a therapeutic target. FASEB J 4:2441–2452
7. White EL, Ross LJ, Cunningham A, Escuyer V (2004) Cloning, expression and characterization of *Mycobacterium tuberculosis* dihydrofolate reductase. FEMS Microbiol Lett 232:101–105
8. Sardarian A, Douglas KT, Read M, Sims PFG, Hyde JE, Chitnumsub P, Sirawaraporn R, Sirawaraporn W (2003) Pyrimethamine analogues as strong inhibitors of double and quadruple mutants of dihydrofolate reductase in human malaria parasites. Org Biomol Chem 1:960–964

9. Hekmat-Najad M, Rathod PK (1997) *Plasmodium falciparum*: kinetic interactions of WR99210 with pyrimethamine-sensitive and pyrimethamine-resistant dihydrofolate reductase. Exp Parasitol 87:222–228
10. Wiktor SZ, Sassan-Morokro M, Grant AD, Abouya L, Karon JM, Marice C, Djomand G, Ackah A, Domoua K, Kadio A, Yapi A, Combe P, Tossou O, Roels TH et al (1999) Efficacy of trimethoprim-sulfamethoxazole prophylaxis to decrease morbidity and mortality in HIV-1 infected patients with tuberculosis in Abijian, Cote d'Ivoire: a randomized control trial. Lancet 353:1469–1475
11. Argyrou A, Vetting MW, Aladegbamil B, Blanchard JS (2006) *Mycobacterium tuberculosis* dihydrofolate reductase is a target for isoniazid. Nat Struct Mol Biol 13(5):408–413
12. Li R, Sirawaraporn R, Chitnumsub P, Sirawaraporn W, Wooden J, Athappilly F, Turley S, Hol WG (2000) Three-dimensional structure of *M. tuberculosis* dihydrofolate reductase reveals opprtunities for the design of novel tuberculosis drugs. J Mol Biol 295:307–323
13. Berman HM, Westbrook J, Feng Z, Gilliland G, Bhat TN, Weissig H, Shindyalov IN, Bourne PE (2000) The protein data bank. Nucleic Acids Res 28:235–242
14. Cody V, Galitsky N, Luft JR, Pangborn W, Rosowsky A, Blakley RL (1997) Comparison of two independent crystal structures of human dihydrofolate reductase ternary complexes reduced with nicotinamide adenine dinucleotide phosphate and the very tight binding inhibitor PT523. Biochemistry 36:4399–4411
15. Johnson JM, Meiering EM, Wright JE, Pardo J, Rosowsky A, Wagner G (1997) NMR solution structure of the antitumor compound PT523 and NADPH in the ternary complex with human dihydrofolate reductase. Biochemistry 36:13897–13903
16. da Cunha EFF, Ramalho TC, Reynolds RC (2008) Binding mode analysis of 2,4-diamino-5-methyl-5-deaza-6-substituted pteridines with *Mycobacterium tuberculosis* and human dihydrofolate reductase. J Biomol Struct Dyn 25(4):377–385
17. Otvos L (2008) Peptide-based drug design: here and now. Pept-Based Drug Des 494:1–8
18. Accelrys Software Inc (2003) Cerius2 modeling environment, release 4.7. Accelrys Software Inc, San Diego
19. Brooks BR, Bruccoleri RE, Olafson BD, States DJ, Swaminathan S, Karplus M (1983) CHARMM: a program for macromolecular energy, minimization, and dynamics calculations. J Comput Chem 4:187–217
20. Momany FA, Rone R (1992) Validation of the general purpose QUANTA ®3.2/CHARMm® force field. J Comput Chem 13:888–900
21. Wu G, Robertson DH, Brooks CL, Vieth M (2003) Detailed analysis of grid-based molecular docking: a case study of CDOCKER—a CHARMm-based MD docking algorithm. J Comput Chem 24:1549–1562
22. Hamdouchi C, Zhong B, Mendoza J, Collins E, Jaramillo C, Diego JE, Robertson D, Spencer CD, Anderson BD, Watkins SA, Zhang F, Brooks HB (2005) Structure-based design of a new class of highly selective aminoimidazo[1,2-a]pyridine-based inhibitors of cyclin dependent kinases. Bioorg Med Chem Lett 15:1943–1947
23. Böhm HJ (1994) The development of a simple empirical scoring function to estimate the binding constant for a protein-ligand complex of known three-dimensional structure. J Comput Aided Mol Des 8:243–256
24. Böhm HJ (1994) On the use of LUDI to search the fine chemicals directory for ligands of proteins of known three-dimensional structure. J Comput Aided Mol Des 8:623–632
25. Böhm HJ (1998) Prediction of binding constants of protein ligands: a fast method for the prioritization of hits obtained from de novo design or 3D database search programs. J Comput Aided Mol Des 12:309–323
26. Wang R, Lu Y, Wang S (2003) Comparative evaluation of 11 scoring functions for molecular docking. J Med Chem 46:2287–2303
27. Berendsen HJC, Postma JPM, DiNola A, Gunsteren WFvan , Haak JR (1984) Molecular dynamics with coupling to an external bath. J Chem Phys 81:3684–3690
28. Subba Rao G, Vijayakrishnan R, Kumar M (2008) Structure-based design of a novel class of potent inhibitors of InhA, the Enoyl acyl carrier protein reductase from *Mycobacterium tuberculosis*: a computer modelling approach. Chem Biol Drug Des 72:444–449
29. DeLano WL (2002) The PyMOL molecular graphics system. http://www.pymol.org